

6 May, 2002  
 HIP-2002-23/TH  
 hep-ph/0205048

## A PERTURBATIVE QCD ANALYSIS OF CHARGED-PARTICLE DISTRIBUTIONS IN HADRONIC AND NUCLEAR COLLISIONS

K.J. Eskola<sup>1</sup> and H. Honkanen<sup>2</sup>

*Department of Physics, University of Jyväskylä,  
 P.O.Box 35, FIN-40351 Jyväskylä, Finland*

*Helsinki Institute of Physics,  
 P.O.Box 64, FIN-00014 University of Helsinki, Finland*

### Abstract

We compute the distributions of charged particles at large transverse momenta in  $p\bar{p}(p)$ ,  $pA$  and  $AA$  collisions in the framework of perturbative QCD, by using collinear factorization and the modern PDFs and fragmentation functions. At the highest cms-energies the shape of the spectra measured in  $p\bar{p}(p)$  collisions at large  $q_T$  can be well explained. The difference between the data and the lowest-order computation is quantified in terms of a constant  $K$ -factor for each energy. The  $K$ -factor is found to systematically decrease with growing  $\sqrt{s}$ . Also a lower limit for the partonic transverse momentum,  $p_0$ , is extracted for each  $\sqrt{s}$  based on the comparison with the measurements. A systematic increase of  $p_0$  as a function of  $\sqrt{s}$  is found. Nuclear effects in the charged-particle spectra in  $pA$  and  $AA$  collisions at RHIC and LHC are studied in the framework of collinear factorization by applying the EKS98 nuclear corrections to the parton distributions. The nuclear effects are shown to mostly enhance the computed spectra. A comparison with the recent PHENIX data from central and peripheral Au+Au collisions at RHIC is done.

---

<sup>1</sup>kari.eskola@phys.jyu.fi

<sup>2</sup>heli.honkanen@phys.jyu.fi

# 1 Introduction

Perturbative QCD (pQCD) and collinear factorization has been shown to be successful in explaining the production of observable jets in  $p\bar{p}$  collisions [1, 2]. The elements in such calculations are the parton distribution functions (PDF) which contain non-perturbative input at some initial scale  $Q_0^2$ , perturbatively computed cross sections for parton-parton scatterings, and the infrared-safe measurement functions which determine the cross section to be computed. For the same energies it is, however, surprisingly difficult to predict inclusive one-particle distributions of charged hadrons in hadron-hadron collisions from perturbative QCD, even at large cms-energies  $\sqrt{s} \gtrsim 100$  GeV and  $p_T \gg \Lambda_{\text{QCD}}$ , where the perturbation theory should work very well.

In the framework of collinear factorization, the inclusive charged-particle transverse momentum spectra can be computed by convoluting the inclusive production of a parton  $k$  further with the corresponding fragmentation function of  $k$  into a hadron  $h$ ,  $D_{k \rightarrow h}$ . Schematically

$$d\sigma^{pp \rightarrow h+X} = \sum_{ijk} f_i(x_1, Q^2) f_j(x_2, Q^2) \otimes \hat{\sigma}^{ij \rightarrow k+x}(x_1, x_2, Q^2, \alpha_s(\mu^2)) \otimes D_{k \rightarrow h}(z, \mu_F^2), \quad (1)$$

where the partonic cross sections  $\hat{\sigma}^{ij \rightarrow k+x}$  are expressed as a power expansion in  $\alpha_s(\mu)$ . The factorization scale is denoted by  $Q$ , the renormalization scale by  $\mu$ , and the fragmentation scale by  $\mu_F$ . State-of-the-art calculations where next-to-leading order (NLO) partonic cross sections and NLO PDF are incorporated with NLO fragmentation functions [3, 4] extracted from  $e^+e^-$  collisions can be found in [5, 6]. While in these calculations the NLO results are well compatible with the measured cross sections [7, 8, 9] at large transverse momenta, the shape of the data is generally not well reproduced at  $q_T \lesssim 5$  GeV. This can be thought to be as a consequence of the fact that the fragmentation functions of gluons are not sufficiently constrained by the  $e^+e^-$  data, or that the effects of intrinsic  $k_T$  both in the fragmentation functions and in the PDF are neglected. Especially at lower cms-energies the  $k_T$ -effects are expected to become important, and phenomenological approaches studying this problem starting from  $pp$  collisions at  $\sqrt{s} \sim 20$  GeV have been developed e.g. in [10, 11] based on the lowest-order (LO) pQCD approach.

In this paper, we will not make an effort to perform a NLO computation of the charged-particle transverse momentum spectra, or to invoke a phenomenological model for the intrinsic  $k_T$ -effects. Instead, we compute the inclusive production of charged particles in LO but strictly remaining within the collinearly factorized approach, supplementing the computation only with a constant  $K$ -factor but no other phenomenological factors. We show that the shape of the computed transverse momentum distributions agrees reasonable (surprisingly?) well with the measured ones in most cases. Emphasizing the highest values of transverse momenta measured at each cms-energy, we determine the  $K$ -factors ( $K \equiv d\sigma_{\text{exp}}^h/d\sigma_{\text{LO}}^h$ ) based on a  $\chi^2$  fit to the data. A systematic decrease of  $K$  with growing cms-energy is found.

Particle production in hadronic and nuclear collisions is often modelled in terms of minijet production above some transverse momentum cut-off  $p_0$ , supplemented with a nonperturbative component for  $p_T \leq p_0$  [12, 13, 14]. The lower limit of partonic transverse momentum needs to be phenomenologically determined from the measurements. This is done e.g. using the total and inelastic cross sections in  $p\bar{p}$  and  $pp$  scatterings in context with eikonal models [12, 15]. The charged-particle spectra measured at midrapidity, however, offer another independent way of obtaining constraints for the cut-off scale. Our second goal in this paper is to try to find lower limits for  $p_0$  based on the comparison of the computed and measured  $p_T$  distributions of charged hadrons. A systematic increase of  $p_0$  as a function of  $\sqrt{s}$  is found.

Our third goal is to study the magnitude of the nuclear effects in high- $p_T$  hadron production in  $pA$  and  $AA$  collisions at RHIC and LHC energies by strictly keeping the framework of collinear factorization and DGLAP evolution. For doing this we apply the EKS98 nuclear modifications [16] to the PDF, and investigate the relative difference between  $AA$  collisions and the corresponding  $pp$  collisions. Both RHIC and LHC energies are studied. We show that the pQCD spectra in central Au+Au collisions at RHIC at  $q_T \lesssim 10$  GeV are enhanced by the nuclear effects at most by 15%.

The fourth and final goal of the present paper is to compare the computed pQCD spectra of charged hadrons to the very exciting recent data from RHIC measured by PHENIX [17]. To obtain the absolute normalization for the spectra, we need to extract the  $K$ -factor for  $\sqrt{s} = 130$  GeV based on the obtained behaviour  $K(\sqrt{s})$ . Two centrality classes are studied. The more peripheral one is found to be consistent with  $pp$  collisions, while in the 0...10% central sample, the computed transverse momentum spectra systematically lie above the data - especially at the highest transverse momenta, where the emphasis of our approach is.

The paper is organized as follows. In Sec. 2 we present the formulae for the computed pQCD cross sections in detail. Sec. 3 explains how the  $K$ -factors are extracted and summarizes the  $p\bar{p}(p)$  results. In Sec. 4 the study is extended to nuclear collisions. Sec. 5 contains the comparison with the PHENIX data. Discussion is given in Sec. 6.

## 2 The formulae

The formulae for computing inclusive charged-particle production in LO pQCD are given below. In LO, the partons are produced back-to-back in the transverse plane according to the differential cross section

$$\frac{d\sigma^{AB \rightarrow kl+X}}{dp_T^2 dy_1 dy_2} = \sum_{ij} x_1 f_{i/A}(x_1, Q^2) x_2 f_{j/B}(x_2, Q^2) \frac{d\hat{\sigma}^{ij \rightarrow kl}}{d\hat{t}}(\hat{s}, \hat{t}, \hat{u}) \quad (2)$$

where  $A$  and  $B$  denote the colliding hadrons or nuclei. The rapidities of the final state partons  $k$  and  $l$  are labelled by  $y_1$  and  $y_2$ , and transverse momentum of each parton by

$p_T$ . The fractional momenta of the colliding partons  $i$  and  $j$  are  $x_{1,2} = \frac{p_T}{\sqrt{s}}(e^{\pm y_1} + e^{\pm y_2})$ , i.e. the incoming partons are collinear with the beams. The parton distributions are obtained from the CERN-PDFLIB library [18], and the factorization scale is  $Q \sim p_T$ . The Mandelstam variables for the subprocesses are denoted by  $\hat{s}, \hat{t}$  and  $\hat{u}$ . In LO, the partonic cross sections are  $d\hat{\sigma}/d\hat{t} \sim \alpha_s^2(\mu^2)$ . The 1-loop expression for the strong coupling constant is used here, so

$$\alpha_s(\mu^2) = \frac{12\pi}{(33 - 2N_f) \log(\mu^2/\Lambda_{\text{QCD}}^{(N_f-2)})}, \quad (3)$$

where  $\mu \sim p_T$  is the renormalization scale. In the present study all partons are considered massless and the number of active flavours,  $N_f = 5, 4, 3$  below the corresponding threshold scales  $Q_6 = m_t = 174$  GeV,  $Q_5 = m_b = 4.5$  GeV and  $Q_4 = m_c = 1.5$  GeV. For  $N_f = 4$ , we will use the  $\Lambda_{\text{QCD}}^{(4)}$  as given by PDFLIB [18] for the chosen set of parton distributions. The change of  $\Lambda_{\text{QCD}}^{(N_f)}$  is computed by requiring matching of  $\alpha_s$  at the threshold scales. The cross sections for the eight different partonic subprocesses can be found e.g. in [19].

Inclusive cross section for production of a parton of a flavour  $f$  and a rapidity  $y_f$  is obtained by integrating over one of the rapidities in Eq. (2) and keeping track of the parton flavours [20],

$$\begin{aligned} \frac{d\sigma^{AB \rightarrow f+X}}{dp_T^2 dy_f} &= \int dy_1 dy_2 \sum_{\langle kl \rangle} \frac{d\sigma^{AB \rightarrow kl+X}}{dp_T^2 dy_1 dy_2} [\delta_{kf} \delta(y_f - y_1) + \delta_{lf} \delta(y_f - y_2)] \frac{1}{1 + \delta_{kl}} \quad (4) \\ &= \int dy_2 \sum_{\langle ij \rangle \langle kl \rangle} \frac{1}{1 + \delta_{kl}} \frac{1}{1 + \delta_{ij}} \times \\ &\quad \times \left\{ x_1 f_{i/A}(x_1, Q^2) x_2 f_{j/B}(x_2, Q^2) \left[ \frac{d\hat{\sigma}^{ij \rightarrow kl}}{d\hat{t}}(\hat{s}, \hat{t}, \hat{u}) \delta_{fk} + \frac{d\hat{\sigma}^{ij \rightarrow kl}}{d\hat{t}}(\hat{s}, \hat{u}, \hat{t}) \delta_{fl} \right] \right. \\ &\quad \left. + x_1 f_{j/A}(x_1, Q^2) x_2 f_{i/B}(x_2, Q^2) \left[ \frac{d\hat{\sigma}^{ij \rightarrow kl}}{d\hat{t}}(\hat{s}, \hat{u}, \hat{t}) \delta_{fk} + \frac{d\hat{\sigma}^{ij \rightarrow kl}}{d\hat{t}}(\hat{s}, \hat{t}, \hat{u}) \delta_{fl} \right] \right\} \quad (5) \end{aligned}$$

where the summations run over the pairs, i.e.  $\langle kl \rangle, \langle ij \rangle = gg, gq, g\bar{q}, qq, q\bar{q}, q\bar{q}, \bar{q}\bar{q}$ , ( $q = u, d, s, \dots$ ) without a mutual change.

For inclusive hadron production through fragmentation of the parton  $f$ , let us define the transverse momentum of a hadron  $h$  be  $q_T$ , its transverse mass  $m_T$  and rapidity  $y$ . We define the fraction  $z$  to be the ratio of the energy of the hadron and the energy of the parton  $f$  from which the hadron originates:  $z = E_h/E_f$ . The hadron is considered to be produced collinearly with the parton. With these definitions the partonic variables become related to the hadronic ones through the relations

$$m_T \cosh y = z p_T \cosh y_f \quad \text{and} \quad m_T \sinh y = q_T \sinh y_f. \quad (6)$$

The inclusive cross section for hadron production can then be written as

$$\frac{d\sigma^{AB \rightarrow h+X}}{dq_T^2 dy} = \frac{d\sigma^{AB \rightarrow h+X}}{dm_T^2 dy} = K(\sqrt{s}) \sum_f \int_{p_0^2} dp_T^2 dy_f \frac{d\sigma^{AB \rightarrow f+X}}{dp_T^2 dy_f} \int_0^1 dz D_{f \rightarrow h}(z, \mu_F^2) \times \delta(m_T^2 - M_T^2(q_T, y_f, z)) \delta(y - Y(q_T, y_f, z)) \quad (7)$$

where the transverse mass and rapidity of the hadron are expressed in terms of the integration variables as

$$M_T^2(p_T, y_f, z) = (zp_T)^2 + m^2 \tanh^2 y_f, \quad Y(p_T, y_f, z) = \text{arsinh}(\frac{q_T}{m_T} \sinh y_f). \quad (8)$$

For the fragmentation functions  $D_{f \rightarrow h}$  we shall use the set KKP [4] which is the latest one. The fragmentation scale is  $\mu_F \sim q_T$ .

One of the tasks below will be to determine the  $K$ -factor based on charged-hadron production measured in  $p\bar{p}(p)$  collisions at collider energies in the range  $\sqrt{s} = 63 \dots 1800$  GeV. The  $K$ -factor thus effectively accounts for the higher-order effects in the partonic cross sections, in the running coupling, in the parton distributions and fragmentation functions, and also for the possible intrinsic transverse momentum effects in the parton showers both in the initial and in the final state. We shall analyze the  $\sqrt{s}$  dependence of  $K$ , in particular.

The parameter  $p_0$  in Eq. (7) is the smallest transverse momentum of parton scatterings allowed. For models with semi-hard parton production, this parameter plays a key role. We shall also discuss the lower limit for  $p_0$  for each  $\sqrt{s}$ .

For completeness, we write down the cross section above in an explicit form, which can be numerically evaluated in a straightforward manner. Performing the integrations over  $p_T^2$  and  $y_f$  in Eq. (7) gives

$$\frac{d\sigma^{AB \rightarrow h+X}}{dq_T^2 dy} = K(\sqrt{s}) \cdot J(m_T, y) \sum_f \int \frac{dz}{z^2} D_{f \rightarrow h}(z, \mu_F^2) \frac{d\sigma^{AB \rightarrow f+X}}{dp_T^2 dy_f} \Big|_{p_T^2, y_f} \quad (9)$$

$$= K(\sqrt{s}) \cdot J(m_T, y) \int \frac{dz}{z^2} \int dy_2 \sum_{\langle ij \rangle \langle kl \rangle} \frac{1}{1 + \delta_{kl}} \frac{1}{1 + \delta_{ij}} \times \\ \left\{ x_1 f_{i/A}(x_1, Q^2) x_2 f_{j/B}(x_2, Q^2) \left[ \frac{d\hat{\sigma}^{ij \rightarrow kl}}{dt}(\hat{t}, \hat{u}) D_{k \rightarrow h}(z, \mu_F^2) + \frac{d\hat{\sigma}^{ij \rightarrow kl}}{dt}(\hat{u}, \hat{t}) D_{l \rightarrow h}(z, \mu_F^2) \right] \right. \\ \left. + x_1 f_{j/A}(x_1, Q^2) x_2 f_{i/B}(x_2, Q^2) \left[ \frac{d\hat{\sigma}^{ij \rightarrow kl}}{dt}(\hat{u}, \hat{t}) D_{k \rightarrow h}(z, \mu_F^2) + \frac{d\hat{\sigma}^{ij \rightarrow kl}}{dt}(\hat{t}, \hat{u}) D_{l \rightarrow h}(z, \mu_F^2) \right] \right\} \quad (10)$$

where the partonic cross section is evaluated at

$$p_T = \frac{q_T}{z} J(m_T, y), \quad y_f = \text{arsinh}(\frac{m_T}{q_T} \sinh y) \quad (11)$$

and where

$$J(m_T, y) = \left(1 - \frac{m^2}{m_T^2 \cosh^2 y}\right)^{-1/2}. \quad (12)$$

The integration region for  $y_2$ ,  $-\log(\sqrt{s}/p_T - e^{-y_f}) \leq y_2 \leq \log(\sqrt{s}/p_T - e^{y_f})$ , is over the whole phase space, whereas that for  $z$ ,

$$\frac{2m_T}{\sqrt{s}} \cosh y \leq z \leq \min \left[ 1, \frac{q_T}{p_0} J(m_T, y) \right], \quad (13)$$

is affected by the requirement  $p_T \geq p_0$ . In this way, we shall also be able to consider the region  $q_T < p_0$ .

The experiments most often give the cross sections averaged over a pseudorapidity interval  $\Delta\eta$ , defined as

$$\frac{d\sigma_{AB}^h}{dq_T^2 d\eta} \Big|_{\eta \in \Delta\eta} \equiv \frac{1}{\Delta\eta} \int_{\Delta\eta} d\eta \frac{d\sigma_{AB}^h}{dq_T^2 d\eta} = \frac{1}{\Delta\eta} \int_{\Delta\eta} d\eta J(m_T, y)^{-1} \frac{d\sigma_{AB}^h}{dq_T^2 dy}, \quad (14)$$

where  $y = \text{arsinh}(\frac{q_T}{m_T} \sinh \eta)$  and  $J(m_T, y)^{-1} = \partial y / \partial \eta$ , where  $J(m_T, y)$  is the same factor as in Eq. (12).

### 3 The analysis and results for $p\bar{p}(p)$

The approach of collinear factorization and independent fragmentation can be expected to work best at the highest values of  $q_T$  and at the highest cms-energies. We determine  $K$  for each  $\sqrt{s}$  based on the data in the large- $q_T$  region by minimizing the  $\chi^2$ :

$$\chi^2(N) = \sum_{i=1}^N \left( \frac{K\sigma_i^{\text{th}} - \sigma_i^{\text{exp}}}{\Delta_i^{\text{exp}}} \right)^2 \quad (15)$$

where  $\sigma_i^{\text{exp}}$  is the measured cross section at a transverse momentum  $q_{Ti}$ , with a statistical error  $\Delta_i^{\text{exp}}$ . The cross sections computed at  $q_{Ti}$  without the  $K$ -factor, are denoted by  $\sigma_i^{\text{th}}$ . The  $N$  data points included in the fit are counted starting from the highest  $q_T$  measured for each  $\sqrt{s}$ . As will be seen, the  $K$ -factor usually depends on  $N$ .

Since in the region of large  $q_T$  one is sensitive to the (statistical) fluctuations in the experimental data, it would be preferable to include as many data points in the fit as possible (most preferably all points of course). The previous comparisons [5, 6] of the pQCD cross sections with the data indicate, however, that the pQCD results tend to fall somewhat below the data in the region of  $q_T \sim 3 \dots 5$  GeV. Also, the pQCD cross sections clearly become too large at  $q_T \lesssim 1$  GeV, which region is sensitive to the cut-off parameter  $p_0$ . The statistical error bars of the data in the few-GeV region are clearly smaller than those at large- $q_T$ . Thus, if the few-GeV region is included in the fit for the determination of the  $K$ -factor, a bad fit for the large- $q_T$  region results. This can

be seen in Fig. 1 (bottom right), where we plot the  $K$ -factors obtained for the UA1 MIMI data at  $\sqrt{s} = 630$  GeV as a function of the smallest transverse momentum  $q_{TN}$  included in the fit. In the same figure, we also show  $\chi^2/N$  as a quantitative measure of the goodness of the fit.

To circumvent the problems mentioned above, and to make sure that the  $K$ -factor gets determined from the region where the collinearly factorized pQCD approach is supposed to work best, we determine the maximum number of data points that can be included by requiring a good fit,  $\chi^2(N)/N \leq 1$ , at  $q_T \geq q_{TN}$ , and fix the  $K$ -factor based on these  $N$  data points. We estimate the statistical significance of the  $K$ -factor at each  $\sqrt{s}$  by computing an error [21]

$$\Delta_K(N) = \left[ \sum_{i=1}^N (\Delta_i^{\text{exp}})^2 \left( \frac{\partial K}{\partial \sigma_i^{\text{exp}}} \right)^2 \right]^{\frac{1}{2}}. \quad (16)$$

This gives the error bars shown in Fig. 1, lower right. For the UA1 MIMI data we find that  $\chi^2(N)/N \leq 1.0$  at  $q_T \geq 7.988$  GeV, with  $N = 15$ , and  $K = 2.19 \pm 0.11$ .

The  $q_T$  spectrum of charged hadrons in  $p\bar{p}$  at  $\sqrt{s} = 630$  GeV, computed from Eq. (14) by applying the  $K$ -factor determined above, is shown in Fig. 1 (left panel) together with the UA1 MIMI data for  $p + \bar{p} \rightarrow h + X$  ( $h \equiv h^+ + h^-$ ). The sum of charged hadrons always includes pions, kaons and protons. Both the data and the computation are averaged over  $-3.0 < \eta < 3.0$ . Contrary to what perhaps could have been expected, the agreement with the data are relatively good, taking into account that we discuss particle production which extends over 10 orders of magnitude. A more detailed comparison is done in the top right panel of Fig. 1, where we plot the data divided by the computed cross section, together with (relative) statistical error bars of the data. From this figure we can see why large  $\chi^2/N$  follows if the few-GeV region is included in the fit.

Fig. 1 (left and top right) also illustrates how we can estimate the lower limit for the parameter  $p_0$ : we require that the computation must not overshoot the measured cross section in the region  $q_T \geq p_0$ . For this particular data set, we notice that e.g. for  $p_0 = 3$  GeV the computed spectrum remains below the measured one until the very last data point  $q_T = 0.079$  GeV. The value  $p_0 = 1$  GeV in turn would cause an overestimate of the cross section already at  $q_T \sim 2$  GeV. This search procedure leads to a lower limit  $p_0 = 1.8 \dots 2.0$  GeV for  $\sqrt{s} = 630$  GeV.

Sensitivity of the computed cross sections to the choice of the fragmentation scale  $\mu_F$  and to the different sets of parton distributions is studied in Fig. 2 for the UA1 MIMI data. The results are shown for the LO sets CTEQ5 [22], MRST(c-g) [23], GRV98 [24] with the scales  $\mu_F = q_T$  and  $\mu_F = q_T/2$ . Notice that in this figure we have already included the  $K$ -factor which is determined as explained above. The actual value of the  $K$ -factor is always correlated with these choices, and for e.g. CTEQ5 and  $\mu_F = q_T/2$ , we get  $K = 1.76 \pm 0.05$ . We notice that qualitatively the behaviour of the computed results relative to the data is the same as for  $\mu_F = q_T$ . Quantitatively,

$\sqrt{s}/\text{GeV}$	collab.	ref.	syst. err.	$K \pm \Delta K$	$p_0/\text{GeV}$	$q_{TN}/\text{GeV}$	N
63	AFS	[25]	20%	$6.19 \pm 0.58$	-	4.65	2
200	UA1	[7]	15%	$3.42 \pm 0.40$	1.6	3.45	8
500	UA1	[7]	15%	$1.94 \pm 0.20$	1.7	3.35	9
630	UA1/MIMI	[8]		$2.19 \pm 0.11$	1.9	7.988	15
630	CDF	[9]		$1.78 \pm 0.32$	2.0	2.9	2
900	UA1	[7]	15%	$1.09 \pm 0.10$	1.6	4.9	10
1800	CDF	[9]		$1.28 \pm 0.18$	2.2	6.0	5

Table 1: The data sets used in the analysis. Systematic errors are quoted when given. The  $K$ -factors are obtained by requiring a good fit at the high- $q_T$  part of the spectra (see the text), and the error  $\Delta K$  is computed from Eq. (16). Systematic error is not included in the estimates for  $\Delta K$ . Notice that these  $K$ -factors are obtained with the CTEQ5 [22] set of parton distributions, and KKP [4] set of fragmentation functions and with the scale choices  $\mu_F = q_T$ ,  $Q = p_T$ . The values of  $q_{TN}$  and  $N$  are also shown (see the text).

the overall agreement between the computed and measured cross sections could be somewhat improved by optimizing the choice of the fragmentation scale and to some extent also by a choice of the parton distributions (modern sets are to be used, of course). For  $\mu_F = q_T$  the difference between the best and worst fitting curve is  $\sim 20\%$  and for  $\mu_F = q_T/2 \sim 30 - 40\%$ . Although not studied here in more detail, there is also some freedom for choosing the factorization and renormalization scales, which could improve the quality of the overall fit. We do not, however, pursue this study into the direction of optimizing the scale choices based on fits to the data but choose to use  $Q = \mu = p_T$ ,  $\mu_F = q_T$  and the CTEQ5 parton distributions with  $\lambda_{QCD}^{(4)} = 192$  MeV in what follows.

The data sets we study are listed in Table 1. The systematic errors given by the experiments are quoted. Table 1 also summarizes our results for the  $K$ -factors along with their error estimates (systematic errors are not included), and the corresponding  $q_{TN}$  and  $N$ , as well as the obtained values of the lower limits of the cut-off scale  $p_0$ .

Fig. 3 presents the pQCD results with the UA1 MIMI data at  $\sqrt{s} = 630$  GeV averaged over various pseudorapidity intervals. We obtained  $p_0 = 1.9$  GeV and  $K = 2.19 \pm 0.11$  using the data averaged over a range  $|\eta| < 3.0$ . We use these values to decompose the  $q_T$  spectra into pseudorapidity intervals  $|\eta| < 0.6$ ,  $0.6 < |\eta| < 1.2$ ,  $1.2 < |\eta| < 1.8$ ,  $1.8 < |\eta| < 2.4$ ,  $2.4 < |\eta| < 3.0$ . As seen in the figure, these results also agree nicely with the data except for  $1.8 < |\eta| < 2.4$ .

Figs. 4 and 5 show the computed inclusive charged-hadron cross sections for  $p + \bar{p} \rightarrow h + X$  ( $h \equiv h^+ + h^-$ ) at  $\sqrt{s} = 1800$  and 630 GeV together with the CDF data [9]. Averaging is done over a rapidity interval  $|y| < 1.0$ . For  $\sqrt{s} = 1800$  GeV (Fig. 4, bottom right) the distribution of the obtained  $K(q_{TN})$  is nearly flat which indicates a

good agreement with the data. Fig. 4, top right, shows that this is indeed the case. The computed absolute spectrum is shown in the left panel of Fig. 4. The corresponding analysis for  $\sqrt{s} = 630$  GeV is shown in Fig. 5. The agreement with the data seems to be again fairly good although the  $K$ -factor is now fixed only by the last two data points. Note that the data only cover a very limited  $q_T$ -range,  $0.425 < q_T < 3.5$ , so in practice half of the computed spectrum is controlled by  $K$  and the other half by  $p_0$ .

In Figs. 6, 7 and 8 we present the computed  $q_T$ -spectra which correspond to the UA1 data [7] at  $\sqrt{s} = 900, 500$  and  $200$  GeV for  $p + \bar{p} \rightarrow h + X$ , where  $h \equiv (h^+ + h^-)/2$ . The data and the computed spectra are averaged over  $|\eta| < 2.5$ . The systematic error for the data is  $\pm 15\%$  (not shown). The overall agreement with the data for  $\sqrt{s} = 900$  GeV is poor for  $q_T \leq 5$  GeV. A reasonable estimate of  $p_0$  in this case is to take the value which at least reproduces the data at smallest values of  $q_T$ . The result for  $p_0 = 1.6$  GeV with the data is shown in Fig. 6 (left panel). The results for  $\sqrt{s} = 500$  GeV are presented in Fig. 7. The agreement with the data is now reasonable. Also for  $\sqrt{s} = 200$  GeV, shown in Fig. 8, the agreement with the data is again tolerable.

The last (and the smallest  $\sqrt{s}$ ) dataset studied is the AFS data [25] for  $p + p \rightarrow h + X$  ( $h \equiv h^+ + h^-$ ) at  $\sqrt{s} = 63$  GeV, averaged over  $|y| < 0.6$ . The systematic error for the data is  $\pm 20\%$  (not shown). The results are illustrated in Fig. 9. The data are for  $q_T \geq 2.25$  GeV so they cannot be used to determine the value of  $p_0$ .

The  $K$ -factors obtained for different energies are gathered together in Table 1 and in Fig. 10. The inner error bars correspond to the statistical errors  $\Delta K$  computed from Eq. (16), and the outer error bars stand for the systematic errors alone (when available). Except for the UA1 dataset at  $\sqrt{s} = 900$  GeV, the obtained  $K$ -factors decrease systematically with increasing  $\sqrt{s}$ . We also observe that a phenomenological fit of the form  $\log K = A + B \log(\sqrt{s})$  can be justified. As the systematic error bars are not available for all cases, we do not perform such a fit here but note that based on the numbers explicitly given in Table 1, such a fit can be easily performed.

## 4 AA-collisions; nuclear effects

Next we study inclusive charged-hadron production in nuclear collisions. Our emphasis is at the highest cms-energies and at the highest transverse momenta. We do not make an attempt to invoke any model for the Cronin effect which is observed in  $pA$  and  $AA$  collisions at lower energies [26]. Different phenomenological approaches to include the Cronin effect to the pQCD-motivated framework can be found e.g. in [10, 11]. We do not include any modifications of the fragmentation functions, either, which are expected to arise in a very dense medium [27, 28, 29]. Instead, aiming at pQCD cross sections, where additional model details are kept in a minimum, we remain within the collinearly factorized leading-twist framework where the nuclear effects in hadron production arise only from the nuclear modifications of the parton distributions functions.

We define the average number density distribution of a parton flavour  $i$  in a nucleus  $A$  as

$$Af_{i/A}(x, Q^2) \equiv Zf_i^{p/A}(x, Q^2) + (A - Z)f_i^{n/A}(x, Q^2), \quad (17)$$

where the nuclear parton distributions (nPDF) are defined in terms of the corresponding distributions  $f_i$  in the free proton as

$$f_i^{p/A}(x, Q^2) \equiv R_i^A(x, Q^2)f_i(x, Q^2). \quad (18)$$

The nuclear modifications  $R_i^A$  depend on the nucleus, the parton flavour,  $x$ , and through the DGLAP evolution [30] of  $f_i^{p/A}$  also on the scale  $Q^2$ . For  $R_i^A(x, Q^2)$  we use the EKS98-parametrization [16] which is based on a global DGLAP analysis of the nPDF [31]. The distributions in bound neutrons are obtained through isospin symmetry;  $f_{u(\bar{u})}^{n/A} = f_{d(\bar{d})}^{p/A}$  and  $f_{d(\bar{d})}^{n/A} = f_{u(\bar{u})}^{p/A}$ . We do not consider the impact parameter dependence of the nPDF [32, 33] here. Clearly, there are two kinds of nuclear effects in the inclusive nuclear cross sections to be computed: effects due to the nuclear modifications of parton distributions (let us call this shadowing for brevity) and isospin effects.

The inclusive cross sections at  $y = 0$  in  $pA$  and  $AA$  collisions at RHIC and LHC energies are computed from Eq. (10) with the nPDF defined above. Dividing the obtained cross sections by the ones which do not include shadowing but include isospin effects, we obtain the ratios shown in Fig. 11 by the dotted and dotted-dashed curves. In order to see the magnitude of the isospin effects, we compare the nuclear cross sections computed with shadowing and isospin effects against the ones computed for  $pp$ . The resulting ratios,  $R_{pA}(q_T)$  and  $R_{AA}(q_T)$  are shown by the dashed and solid lines. We can see that the isospin effects remain quite small in all cases.

The excess in the ratios  $R_{pA}(q_T)$  and  $R_{AA}(q_T)$  in Fig. 11 is caused by antishadowing in the nPDF (see Fig. 3 of Ref. [16]). The depletion at small values of  $q_T$  is due to shadowing at small  $x$ , and the depletion at larger values of  $q_T$  is due to the EMC effect in the nPDF. The systematics in the location of the excess in  $q_T$ , its magnitude (the height is decreasing with  $\sqrt{s}$ ) is easy to understand by the following argument.

Approximating the partonic cross section roughly by a power-law,  $d\sigma^f/dp_T dy \approx C_f p_T^{-n}$ , and neglecting all masses, Eq. (10) simplifies into

$$\frac{d\sigma^{NN \rightarrow h+X}}{dq_T dy} \approx \sum_{f=g,q,\bar{q}} \frac{C_f}{q_T^n} \int dz z^{n-1} D_{f \rightarrow h}(z, q_T^2), \quad (19)$$

For  $\sqrt{s} = 200$  GeV at  $p_T \sim 10$  GeV, we find  $n \sim 7$  and somewhat less for smaller values of  $p_T$  or larger values of  $\sqrt{s}$ . From Fig. 12 for  $z^6 D(z, q_T^2)$  at  $q_T = 10$  GeV, we observe that the integrand is strongly peaked around  $\bar{z}_f = 0.6 \dots 0.8$ , depending on the flavour of the fragmenting parton. Obviously then  $\int dz z^{n-1} D_{f \rightarrow h}(z) \approx \bar{z}_f^{n-1} D_{f \rightarrow h}(\bar{z}_f, q_T^2)$ . Consider only gluons for simplicity (gluons dominate parton production when  $x \ll 1$  but this is to some extent compensated by the larger fragmentation functions of the quarks). We find that  $d\sigma^h/dq_T dy \sim d\sigma^g/dp_T dy$  where  $p_T \approx q_T/\bar{z}$  with  $\bar{z} \approx 0.6$ .

At  $y = 0$ , the inclusive parton production dominantly probes the region  $x \sim 2p_T/\sqrt{s}$ . The ratio of shadowed and non-shadowed cross sections in Fig. 11 thus behaves as

$$R_{AA}(q_T, \sqrt{s}) \sim [R_g^A(\frac{2q_T}{\bar{z}\sqrt{s}}, \frac{q_T}{\bar{z}})]^p, \quad (20)$$

where, due to the smearing caused by the integration over  $y_2$ , an effective power  $1 < p < 2$  appears. Comparison with Fig. 3 of Ref. [31] for  $R_g^A(x, Q^2)$ , shows that this is indeed the case: the cross-over points in  $R_{AA}(q_T)$  can be traced back to the cross-over points of the ratio  $R_g^A$  in Eq. (20). The decrease in the magnitude of the excess in  $R_{AA}$  with growing  $\sqrt{s}$  is due to the scale evolution of  $R_g^A$ : at higher scales the antishadowing of  $R_g^A$  decreases. Notice also the difference in  $\sqrt{s}$  for  $pA$  and  $AA$  at the LHC.

## 5 Comparison with the PHENIX data

As our final task - armed with the  $\sqrt{s}$  dependence of the  $K$ -factors - we compare our results with the transverse momentum distributions of charged hadrons in Au+Au collisions at  $\sqrt{s} = 130$  GeV at RHIC, which have been recently measured by PHENIX [17]. We consider an average quantity

$$\left\langle \frac{dN^{AA \rightarrow h+X}}{d^2q_T d\eta} \right\rangle_c = \left\langle T_{AA}(b) \frac{d\sigma^{NN \rightarrow h+X}}{d^2q_T d\eta} \right\rangle_c = \langle N_{\text{binary}}^{AA} \rangle_c \frac{1}{\sigma_{\text{in}}^{NN}} \frac{d\sigma^{NN \rightarrow h+X}}{d^2q_T d\eta}, \quad (21)$$

where  $T_{AA}$  is the standard nuclear overlap function,  $NN$  refers to nucleon-nucleon collisions, and  $\langle N_{\text{binary}}^{AA} \rangle_c$  is the average number of binary collisions within the centrality selection  $c$ . In Ref. [17], two centrality classes are given,  $c_1 = 0 \dots 10\%$  and  $c_2 = 60 \dots 80\%$ , along with the estimates  $\langle N_{\text{binary}} \rangle_{c_1} = 905 \pm 96$  and  $\langle N_{\text{binary}} \rangle_{c_2} = 20 \pm 6$  (resulting from a Glauber analysis) and for the inelastic nucleon-nucleon cross section  $\sigma_{\text{in}}^{NN} = 40 \pm 3$  mb. We use these values here. To roughly estimate the impact-parameter dependence of shadowing, we find an effective nucleus  $A_{\text{eff}}$  for which the number of binary collisions in a central  $A_{\text{eff}} A_{\text{eff}}$  collision equals  $\langle N_{\text{binary}} \rangle_{c_2}$ . With  $T_{AA}(0) \approx A^2/\pi R_A^2$ , this leads to  $A_{\text{eff}}^{c_1} \approx 163$  and  $A_{\text{eff}}^{c_2} \approx 9$  for the two centrality classes studied. Shadowing is included according to Eqs. (17) and (18) for  $A = A_{\text{eff}}$ . Thus the nuclear effects for the sample  $c_1(c_2)$  remain within 15(5)% at  $q_T \leq 10$  GeV.

From the systematics of the  $\sqrt{s}$ -dependence of the  $K$ -factors in Fig. 10 it is observed that a simple power-law interpolation between  $\sqrt{s} = 63$  GeV and 200 GeV gives a fair first estimate of the  $K$ -factor at 130 GeV. This results in  $K(\sqrt{s} = 130 \text{ GeV}) = 4.27 \pm 0.18$ . For the error estimate, we have added the statistical and systematic errors of  $K(\sqrt{s} = 200 \text{ GeV})$  in quadrature. Applying this  $K$ -factor, we plot the hadron spectra shown by the solid curves in Fig. 13. For obtaining an estimate of the total relative error (shown in the figure with the dashed lines), we add the relative errors of

$K$ ,  $\langle N_{\text{binary}}^{\text{AA}} \rangle_c$ , and  $\sigma_{\text{in}}^{NN}$  in quadrature. This leads to  $\pm 22\%$  and  $\pm 36\%$  for the central and peripheral cases.

A very good agreement is found between the computed cross sections and the peripheral ( $c_2$ ) data at the highest  $q_T$  measured. The computed spectrum remains also surprisingly close to the measured one at  $q_T \sim 2$  GeV which was the trouble region in the  $p\bar{p}(p)$  case. The estimated error band now covers the most of expected magnitude of the deviations (see Fig. 8). Within the uncertainties estimated, the peripheral Au+Au collisions thus seem to behave effectively as  $NN$  collisions. In central collisions, however, especially towards the largest transverse momenta, the computed spectrum systematically lies above the data. We emphasize that it is in this region that our approach should work the best. It should also be noted that if the Cronin effect for high- $p_T$  parton production becomes more important at central Au+Au collisions than in the peripheral case, it should *increase* the computed cross sections. This would in turn make the difference between the measured and computed spectra even larger from what is seen in Fig. 13. The high- $q_T$  hadron production in central Au+Au collisions thus looks quite different from a straightforward extrapolation of the  $pp$  case.

## 6 Discussion

In this paper we have studied inclusive charged-hadron production in  $p\bar{p}(p)$  collisions at  $\sqrt{s} \geq 63$  GeV in the framework of leading-twist lowest-order perturbative QCD. Modern lowest-order sets of parton distributions and fragmentation functions are used. Comparison with the AFS [25], UA1 [7], UA1 MIMI [8], and CDF [9] data is made, and the difference between the computed and measured spectra is quantified in terms of a factor  $K = d\sigma^{\text{exp}}/d\sigma_{\text{LO}}^{\text{th}}$ . We have extracted the  $K$ -factors and their  $\sqrt{s}$ -dependence from the highest transverse momenta of the measured spectra. A systematic decrease of  $K$  with growing  $\sqrt{s}$  is found. Also error estimates for the obtained  $K$  are given. We emphasize that the values of  $K$  depend on the PDFs, fragmentation functions and the scale choices used. The results of our analysis are useful for further studies of hadron spectra, at cms-energies where no  $pp$  data are so far available.

We have also studied the lower limits for partonic transverse momentum exchange, the cut-off scale  $p_0$ . A systematic increase of  $p_0$  with growing  $\sqrt{s}$  is found and  $p_0 = 1.6 \dots 2.2$  GeV for  $\sqrt{s} = 63 \dots 1800$  GeV. It will be interesting to study the relation of the scales  $p_0$  obtained here to the saturation scales in  $AA$  collisions [34]. For the models with semihard (perturbative) and soft (nonperturbative) components for particle production, our analysis thus suggests a cut-off scale  $p_0$  which increases with  $\sqrt{s}$ . The same observation was also made e.g. in a recent analysis for the HIJING model [15]. Notice that the values of  $p_0$  we obtain are somewhat below those obtained in [15], since here we have described all particle production with the perturbative component only.

Once the  $K$ -factor in each case has been determined, we find the overall agreement between the computed and measured spectra in  $p\bar{p}$  at  $\sqrt{s} \geq 200$  GeV relatively good (except for the UA1 dataset at 900 GeV). In general, the fragmentation functions of gluons are not as well constrained by the  $e^+e^-$  data as those of quarks and antiquarks. In the future it will be very interesting to see whether the agreement of the collinearly factorized cross sections and the data will be improving with new sets of fragmentation functions. It will also be interesting to see how close the results obtained here are with the scale-optimized NLO results [6] at various energies.

The agreement with the  $p\bar{p}$  data at high transverse momenta gives us confidence in that a reference cross section can be obtained by making the extrapolation from  $pp$  to  $AA$  collisions. The computed spectra are compared with the recent measurements by PHENIX [17]. We have shown that in the region  $q_T = 1\dots 10$  GeV for central Au+Au collisions at RHIC the antishadowing effects in parton distributions *enhance* the spectra but only by less than 15%. We have also shown that the isospin effects are small. Using the estimated  $K = 4.27$  for  $\sqrt{s} = 130$  GeV, together with the results from a Glauber analysis of PHENIX, we have computed the inclusive hadron spectra corresponding to the peripheral and central data samples. The results found are very similar to those obtained by PHENIX: the peripheral collisions seem to behave practically as  $pp$  collisions, and the computed spectrum agrees nicely with the data at the largest values of  $q_T$ . In comparison with the data with a 0..10% centrality cut, the computed spectrum is found to systematically lie above the measured spectrum at the highest transverse momenta, where the emphasis of our approach is. An additional Cronin effect, if important at all at this high  $\sqrt{s}$  and large  $q_T$ , can be expected to enhance the computed spectrum and thus enhance the deviation from the data. In order to see the effect even more clearly, we are looking forward to more data points at even higher values of  $q_T$ .

The very dense partonic medium produced (see the initial conditions e.g. in [34]) can be expected to be responsible for the suppression of the high- $q_T$  hadrons [27]. There is an increasing activity to study the fragmentation functions modified by the presence of the partonic medium [28, 29, 35]. Incorporating such modifications into the present analysis will be done next [36]. This procedure focuses on the large- $q_T$  region, where perturbative methods apply. The other extreme case, emphasizing the smaller- $q_T$  region, is hadron production from a fully thermalized system described in terms of relativistic hydrodynamics [37]. It will be very interesting to study how these two regions merge to form the measured spectrum.

## Acknowledgements

We thank V. Karimäki, V. Ruuskanen, C. Salgado and U. Wiedemann for discussions. Financial support from the Academy of Finland, grants no. 50338 and 163065, is gratefully acknowledged.

## References

- [1] S. D. Ellis, Z. Kunszt and D. E. Soper, Phys. Rev. Lett. **69** (1992) 3615 [arXiv:hep-ph/9208249]; Z. Kunszt and D. E. Soper, Phys. Rev. D **46** (1992) 192.
- [2] S. D. Ellis, Z. Kunszt and D. E. Soper, Phys. Rev. Lett. **69** (1992) 1496.
- [3] J. Binnewies, B. A. Kniehl and G. Kramer, Phys. Rev. D **52** (1995) 4947 [arXiv:hep-ph/9503464].
- [4] B. A. Kniehl, G. Kramer and B. Pötter, Nucl. Phys. B **582** (2000) 514 [arXiv:hep-ph/0010289].
- [5] F. M. Borzumati and G. Kramer, Z. Phys. C **67** (1995) 137 [arXiv:hep-ph/9502280].
- [6] P. Aurenche, M. Fontannaz, J. P. Guillet, B. A. Kniehl and M. Werlen, Eur. Phys. J. C **13** (2000) 347 [arXiv:hep-ph/9910252].
- [7] C. Albajar *et al.* [UA1 Collaboration], Nucl. Phys. B **335** (1990) 261.
- [8] G. Bocquet *et al.*, Phys. Lett. B **366** (1996) 434.
- [9] F. Abe *et al.* [CDF Collaboration], Phys. Rev. Lett. **61** (1988) 1819.
- [10] X. n. Wang, Phys. Rev. C **61** (2000) 064910 [arXiv:nucl-th/9812021].
- [11] Y. Zhang, G. Fai, G. Papp, G. G. Barnafoldi and P. Levai, Phys. Rev. C **65** (2002) 034903 [arXiv:hep-ph/0109233]; G. Papp, G. G. Barnafoldi, G. Fai, P. Levai and Y. Zhang, Nucl. Phys. A **698** (2002) 627 [arXiv:nucl-th/0104021].
- [12] X. n. Wang, Phys. Rev. D **43** (1991) 104.
- [13] T. Sjöstrand and M. van Zijl, Phys. Rev. D **36** (1987) 2019.
- [14] K. J. Eskola, K. Kajantie and J. Lindfors, Nucl. Phys. B **323** (1989) 37.
- [15] S. y. Li and X. n. Wang, Phys. Lett. B **527** (2002) 85 [arXiv:nucl-th/0110075].
- [16] K. J. Eskola, V. J. Kolhinen and C. A. Salgado, Eur. Phys. J. C **9** (1999) 61 [arXiv:hep-ph/9807297].
- [17] K. Adcox *et al.* [PHENIX Collaboration], Phys. Rev. Lett. **88** (2002) 022301 [arXiv:nucl-ex/0109003].

- [18] H. Plothow-Besch, Comp. Phys. Comm. **75** (1993) 396; Int. J. Mod. Phys. **A10** (1995) 2901; “PDFLIB: Proton, Pion and Photon Parton Density Functions, Parton Density Functions of the Nucleus, and  $\alpha_s$ ”, Users’s Manual - Version 8.04, W5051 PDFLIB 2000.04.17 CERN-ETT/TT.
- [19] I. Sarcevic, S. D. Ellis and P. Carruthers, Phys. Rev. D **40** (1989) 1446.
- [20] K. J. Eskola and K. Kajantie, Z. Phys. C **75** (1997) 515 [arXiv:nucl-th/9610015].
- [21] William H. Press et al, “Numerical Recipes, The Art of Scientific Computing”, Cambridge University Press 1988, p. 504.
- [22] H. L. Lai *et al.* [CTEQ Collaboration], Eur. Phys. J. C **12** (2000) 375 [arXiv:hep-ph/9903282].
- [23] A. D. Martin, R. G. Roberts, W. J. Stirling and R. S. Thorne, Eur. Phys. J. C **4** (1998) 463 [arXiv:hep-ph/9803445].
- [24] M. Glück, E. Reya and A. Vogt, Eur. Phys. J. C **5** (1998) 461 [arXiv:hep-ph/9806404].
- [25] T. Åkesson *et al.* [Axial Field Spectrometer Collaboration], Nucl. Phys. B **209** (1982) 309.
- [26] D. Antreasyan, J. W. Cronin, H. J. Frisch, M. J. Shochet, L. Kluberg, P. A. Piroue and R. L. Sumner, Phys. Rev. D **19** (1979) 764; J. W. Cronin, H. J. Frisch, M. J. Shochet, J. P. Boymond, R. Mermod, P. A. Piroue and R. L. Sumner, Phys. Rev. D **11** (1975) 3105.
- [27] M. Gyulassy and X. n. Wang, Nucl. Phys. B **420** (1994) 583 [arXiv:nucl-th/9306003].
- [28] X. n. Wang, Z. Huang and I. Sarcevic, Phys. Rev. Lett. **77** (1996) 231 [arXiv:hep-ph/9605213]; M. Gyulassy, P. Levai and I. Vitev, arXiv:nucl-th/0112071.
- [29] C. A. Salgado and U. A. Wiedemann, arXiv:hep-ph/0204221.
- [30] Yu. Dokshitzer, Sov. Phys. JETP **46** (1977) 1649; V.N. Gribov and L. N. Lipatov, Sov. Nucl. Phys. **15** (1972) 438, 675; G. Altarelli, G. Parisi, Nucl. Phys. B **126** (1977) 298.
- [31] K. J. Eskola, V. J. Kolhinen and P. V. Ruuskanen, Nucl. Phys. B **535** (1998) 351 [arXiv:hep-ph/9802350].
- [32] K. J. Eskola, Z. Phys. C **51** (1991) 633.

- [33] V. Emel'yanov, A. Khodinov, S. R. Klein and R. Vogt, Phys. Rev. Lett. **81** (1998) 1801 [arXiv:nucl-th/9805027].
- [34] K. J. Eskola, K. Kajantie, P. V. Ruuskanen and K. Tuominen, Nucl. Phys. B **570** (2000) 379 [arXiv:hep-ph/9909456].
- [35] R. Baier, Y. L. Dokshitzer, A. H. Mueller and D. Schiff, JHEP **0109** (2001) 033 [arXiv:hep-ph/0106347].
- [36] K.J. Eskola *et al.*, work in progress.
- [37] K. J. Eskola, P. V. Ruuskanen, S. S. Räsänen and K. Tuominen, Nucl. Phys. A **696** (2001) 715 [arXiv:hep-ph/0104010].

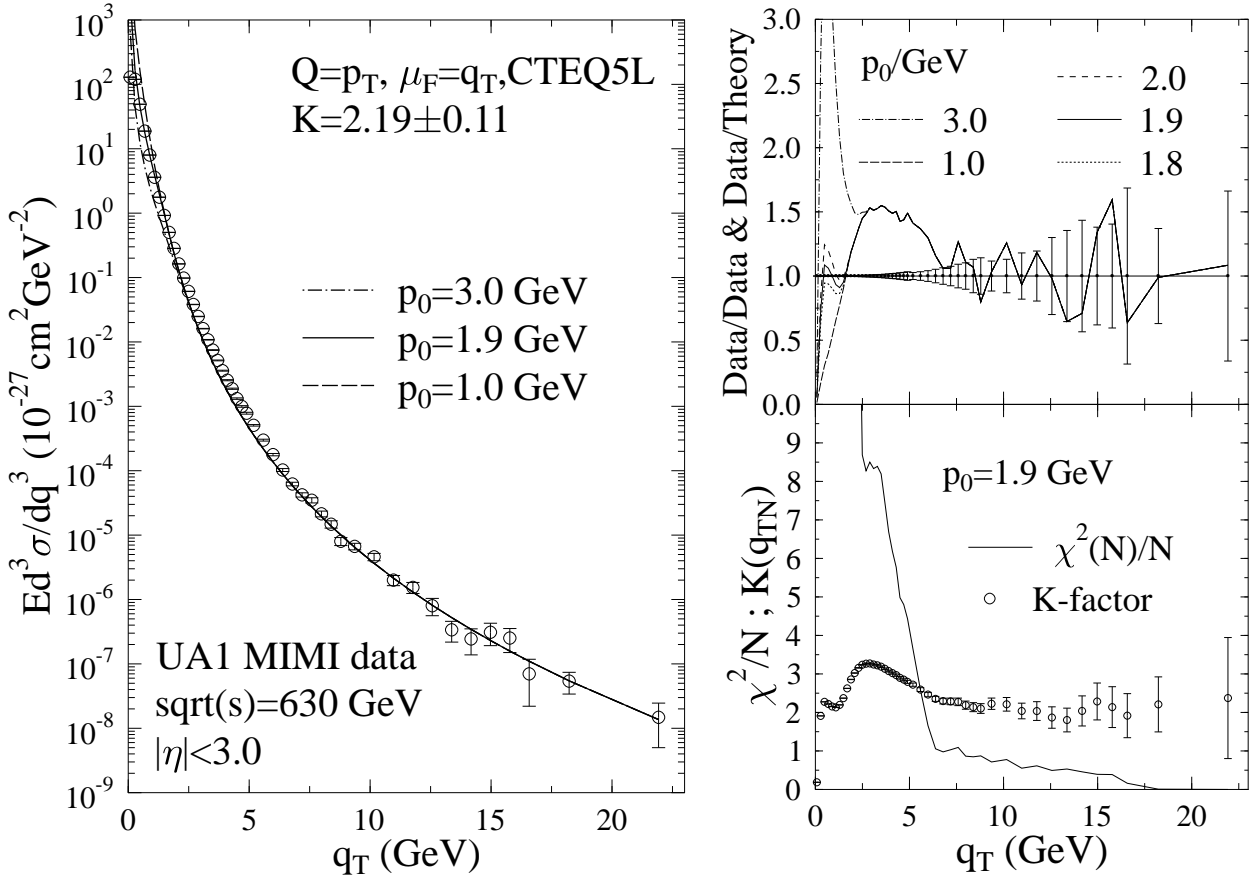


Figure 1: **Left:** Inclusive cross section for charged-hadron production ( $h \equiv h^+ + h^-$ ) in  $p\bar{p}$  collisions at  $\sqrt{s} = 630$  GeV averaged over  $|\eta| < 3.0$ . The LO pQCD prediction with  $K = 2.19$  and scales  $Q = p_T$ ,  $\mu_F = q_T$  and  $p_0 = 1.0, 1.9, 3.0$  GeV is shown by the curves. The data shown with the statistical error bars are from UA1 MIMI [8]. **Top right:** The ratios data-to-data and data-to-theory as a function of transverse momentum for various  $p_0$ . **Bottom right:** The minimized  $\chi^2(N)/N$  (solid curve) and the resulting  $K$ -factor (with error bars) as a function of the smallest transverse momentum,  $q_{TN}$ , included in the fit. The  $K$ -factor is read off from the point where  $\chi^2(N)/N = 1$ . The errors of the  $K$ -factor are computed from Eq. (16).

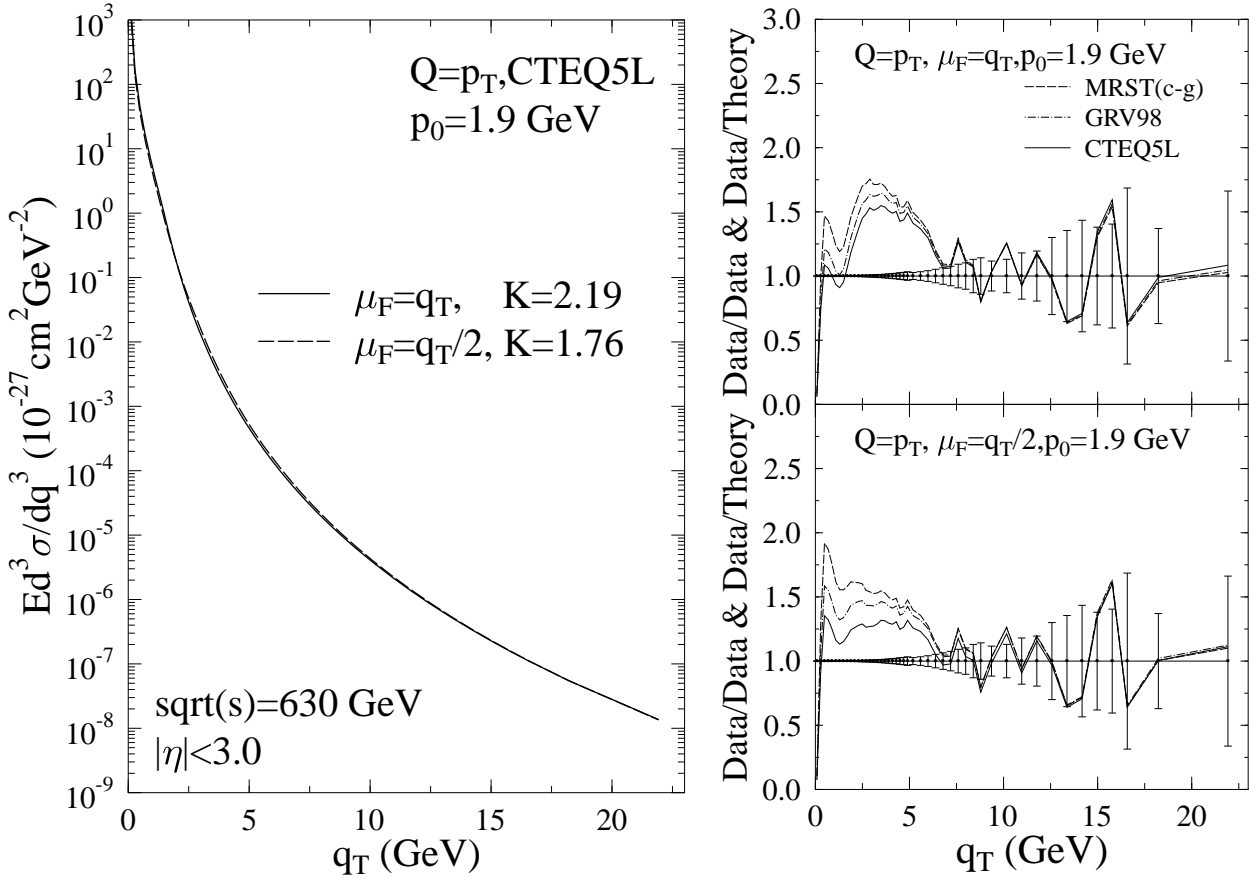


Figure 2: **Left:** An example of the dependence of the inclusive pQCD cross sections (as in Fig. 1) on the choice of the fragmentation scale  $\mu_F$ . Based on the fit to the large- $q_T$  region of the UA1 MIMI data in Fig. 1, we obtain  $K = 2.19 \pm 0.11$  for  $\mu_F = q_T$  and  $K = 1.76 \pm 0.05$  for  $\mu_F = q_T/2$ . The scale  $p_0$  has been fixed to 1.9 GeV and CTEQ5 PDF are used. **Right:** As in the top right panel of Fig. 1 but showing the dependence of the pQCD results on the PDF set. Three different sets are used, and the scales are fixed to  $Q = p_T$  and  $p_0 = 1.9 \text{ GeV}$  in both panels. For the sets CTEQ5L, GRV98 and MRST(c-g), we obtain  $K = 2.19 \pm 0.11, 2.00 \pm 0.10, 2.15 \pm 0.10$  for  $\mu_F = q_T$  (upper panel) and  $K = 1.76 \pm 0.05, 1.53 \pm 0.07, 1.65 \pm 0.08$  for  $\mu_F = q_T/2$  (lower panel).

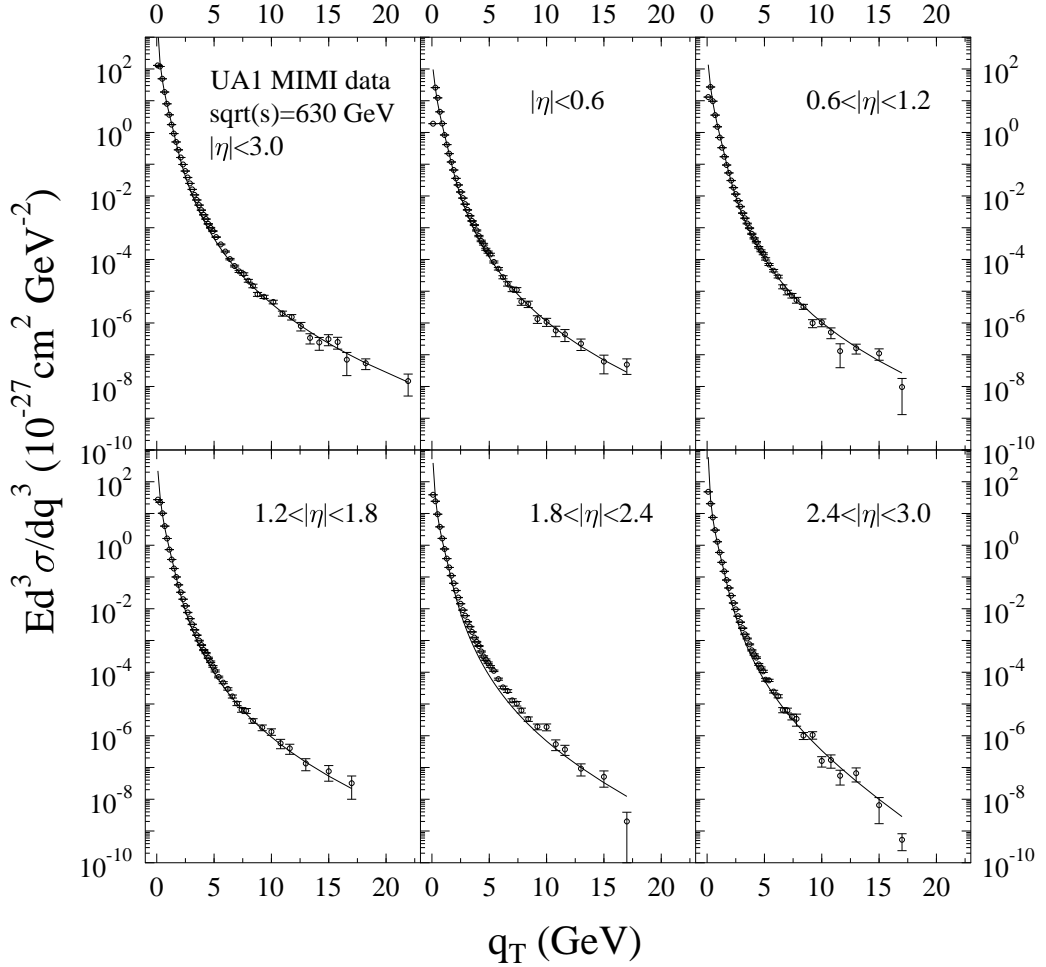


Figure 3: The LO pQCD prediction for the charged-particle spectra in  $p\bar{p}$  collisions at  $\sqrt{s} = 630$  GeV with  $K = 2.19$  and  $p_0 = 1.9$  GeV. The upper left panel corresponds to Fig. 1, in the other panels the pseudorapidity interval  $|\eta| < 3.0$  has been divided into different subintervals. The data are from UA1 MIMI, Ref. [8].

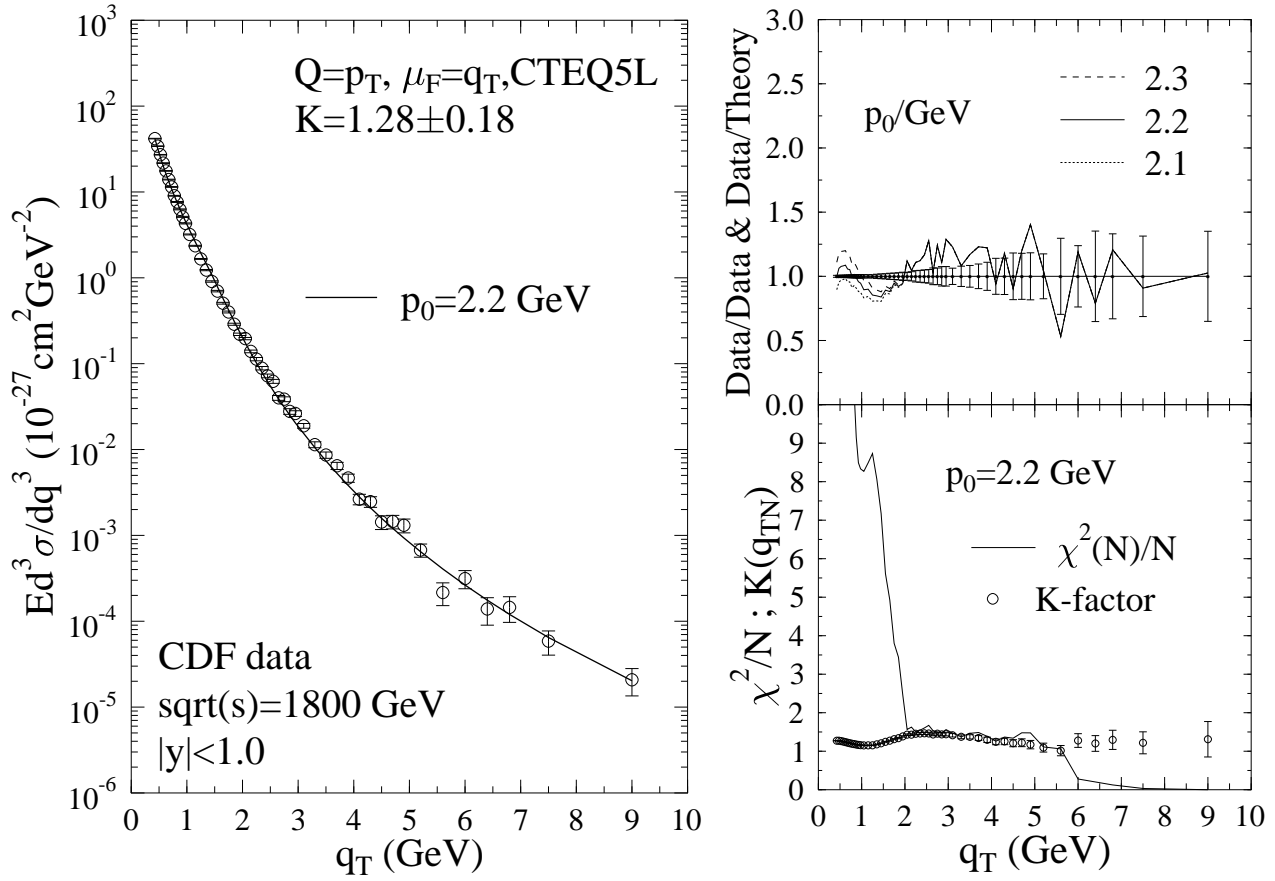


Figure 4: As Fig. 1 but for  $h \equiv (h^+ + h^-)/2$ ,  $\sqrt{s} = 1800 \text{ GeV}$  and  $|y| < 1.0$ . The data are from CDF [9].

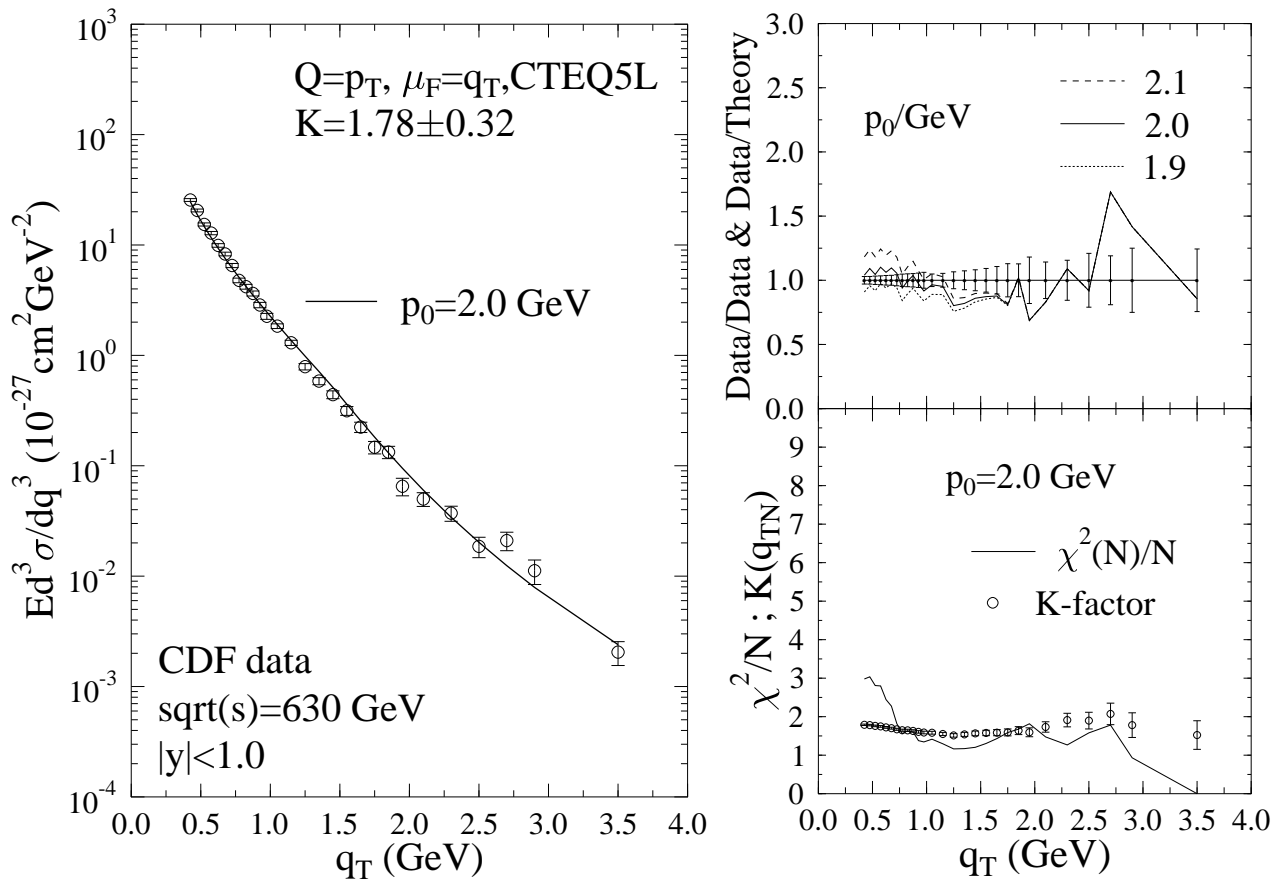


Figure 5: As Fig. 4 but for  $\sqrt{s} = 630 \text{ GeV}$ .

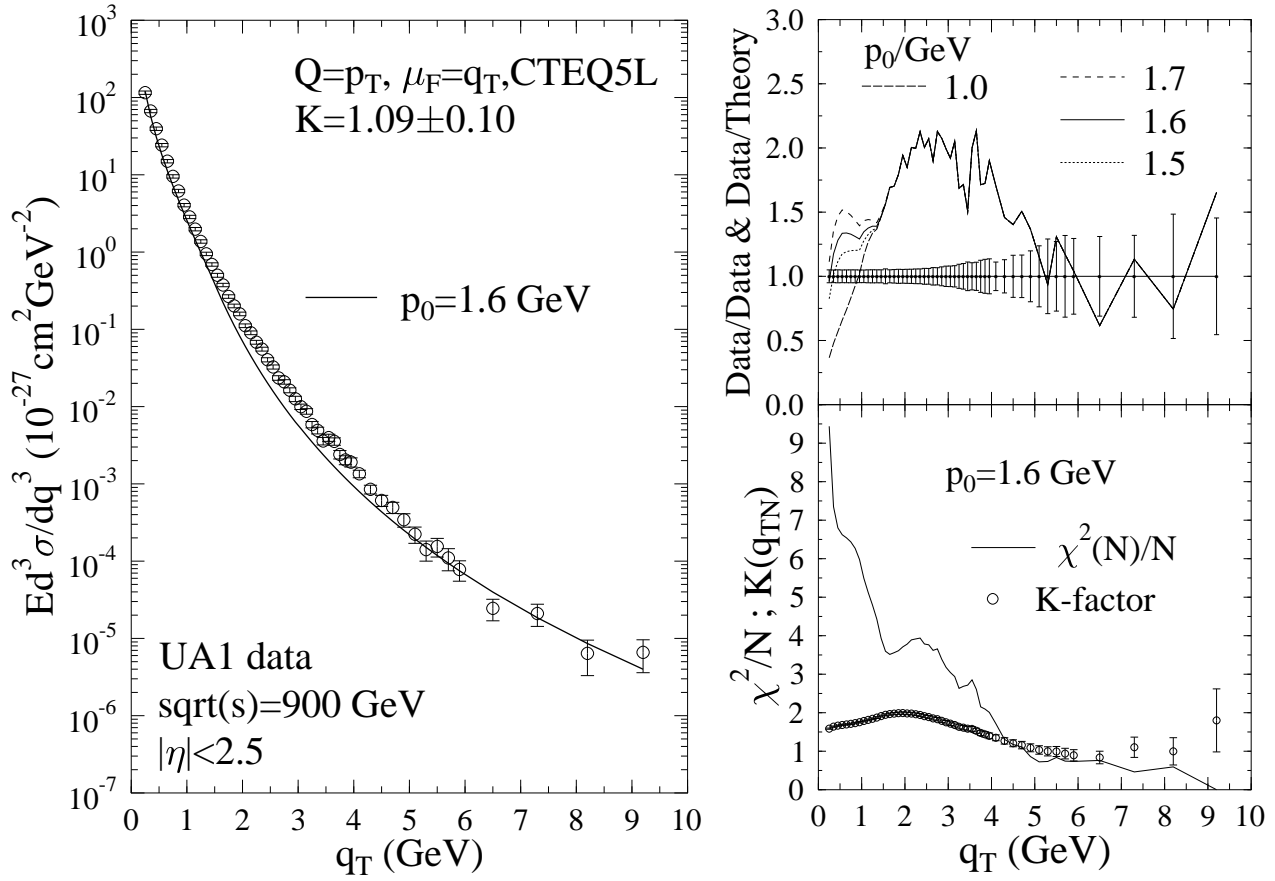


Figure 6: As Fig. 1 but for  $h \equiv (h^+ + h^-)/2$ ,  $\sqrt{s} = 900$  GeV and  $|\eta| < 2.5$ . The data are from UA1 [7].

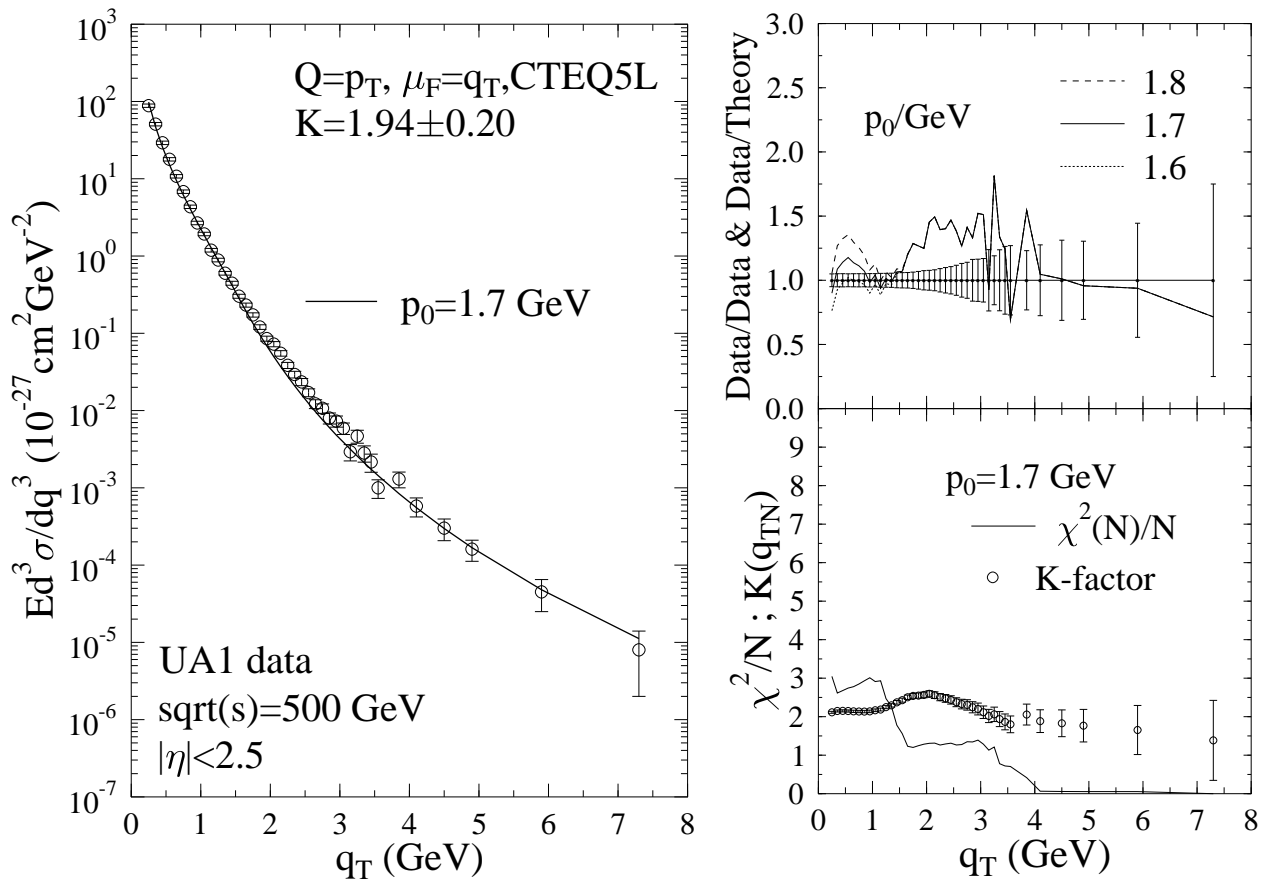


Figure 7: As Fig. 6 but for  $\sqrt{s} = 500 \text{ GeV}$ .

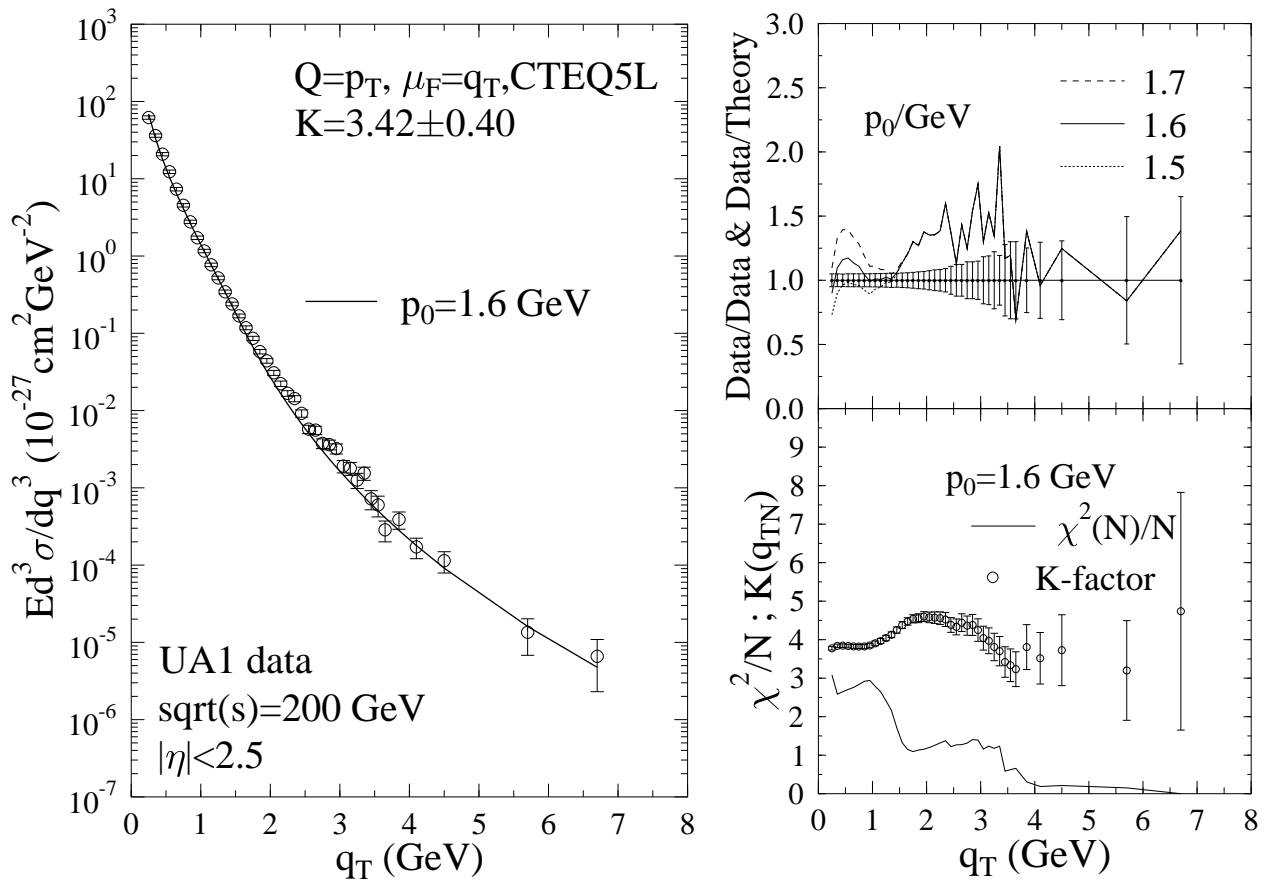


Figure 8: As Fig. 6 but for  $\sqrt{s} = 200 \text{ GeV}$ .

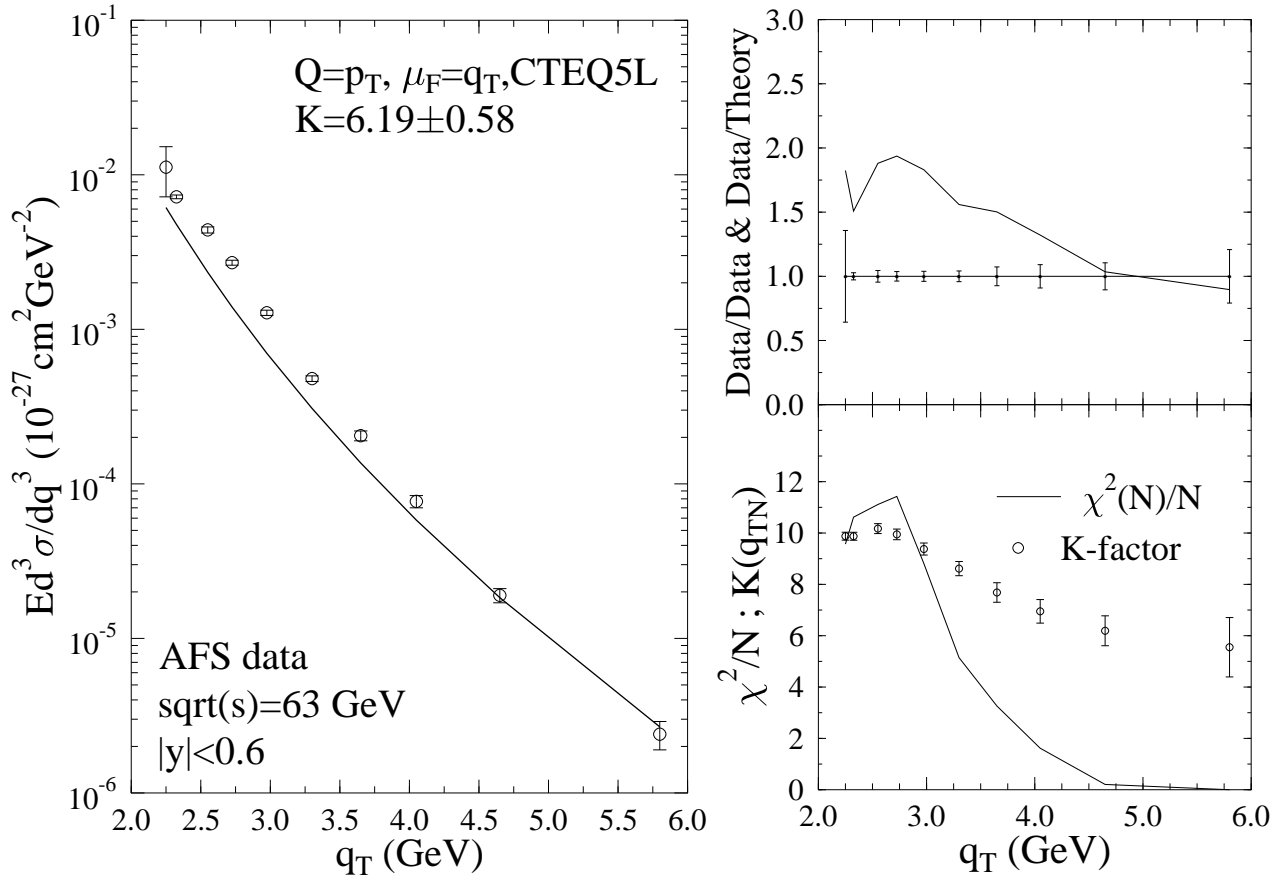


Figure 9: As Fig. 1 but for  $h \equiv h^+ + h^-$ ,  $\sqrt{s} = 63$  GeV and  $|y| < 0.6$ . The data are from [25].

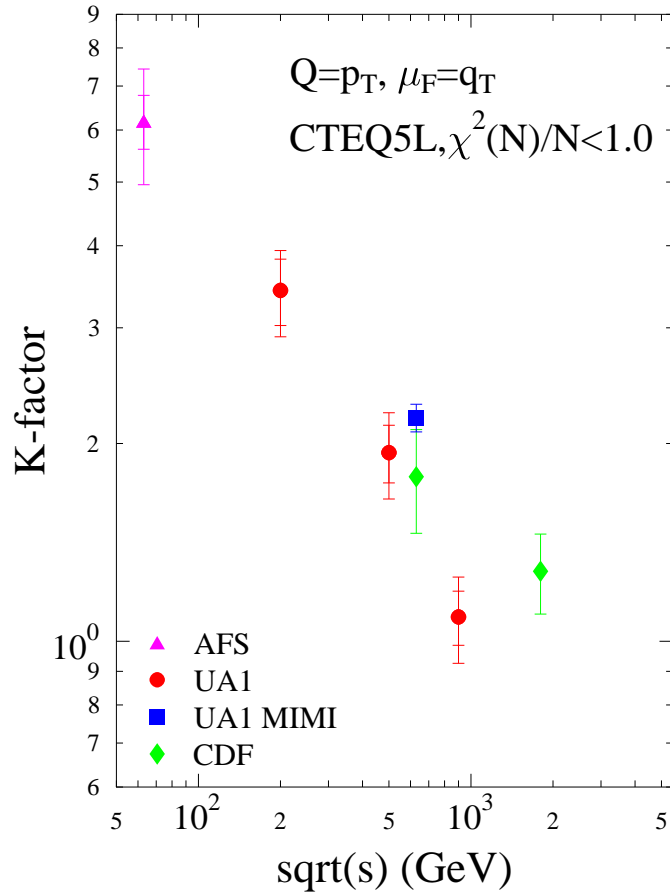


Figure 10: The obtained  $K$ -factors for  $\sqrt{s} = 63, 200, 500, 630, 900, 1800$  GeV. The inner error bars are  $\Delta K$  calculated from Eq. (16) and the outer error bars (when shown) are the reported systematic errors for each data set (see Table 1).

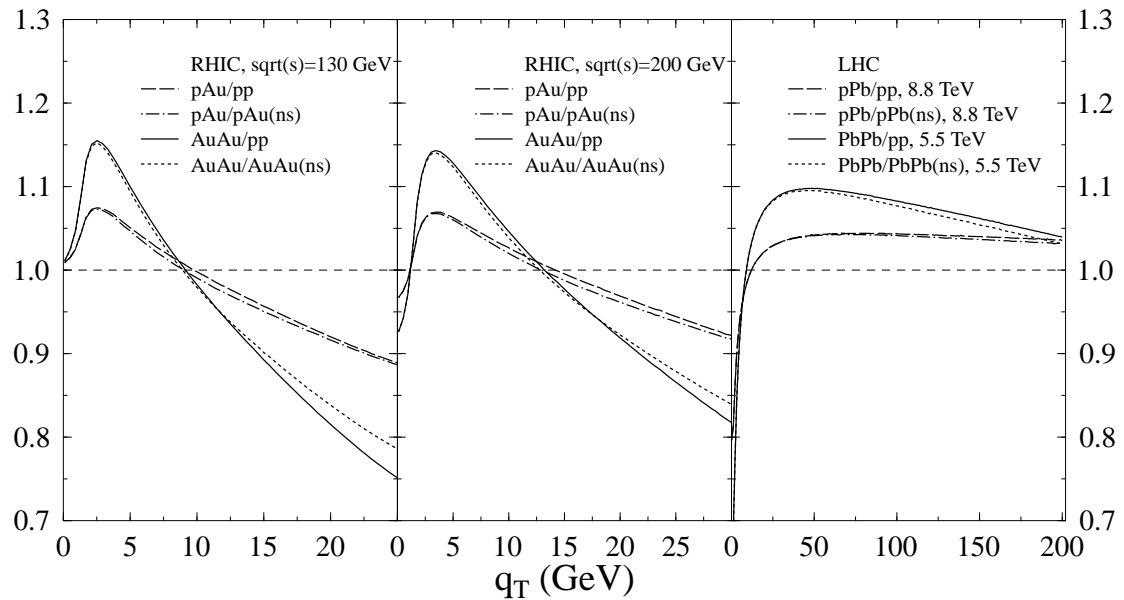


Figure 11: The ratios of transverse momentum spectra of charged hadrons in  $AA(pA)$  collisions relative to  $pp$  collisions and  $AA(pA)$  collisions without shadowing. At RHIC both  $Au+Au$  and  $p+Au$  are at  $\sqrt{s} = 130$  GeV and 200 GeV. At the LHC  $Pb+Pb$  is at  $\sqrt{s} = 5.5$  TeV and  $p+Pb$  at  $\sqrt{s} = 8.8$  TeV.

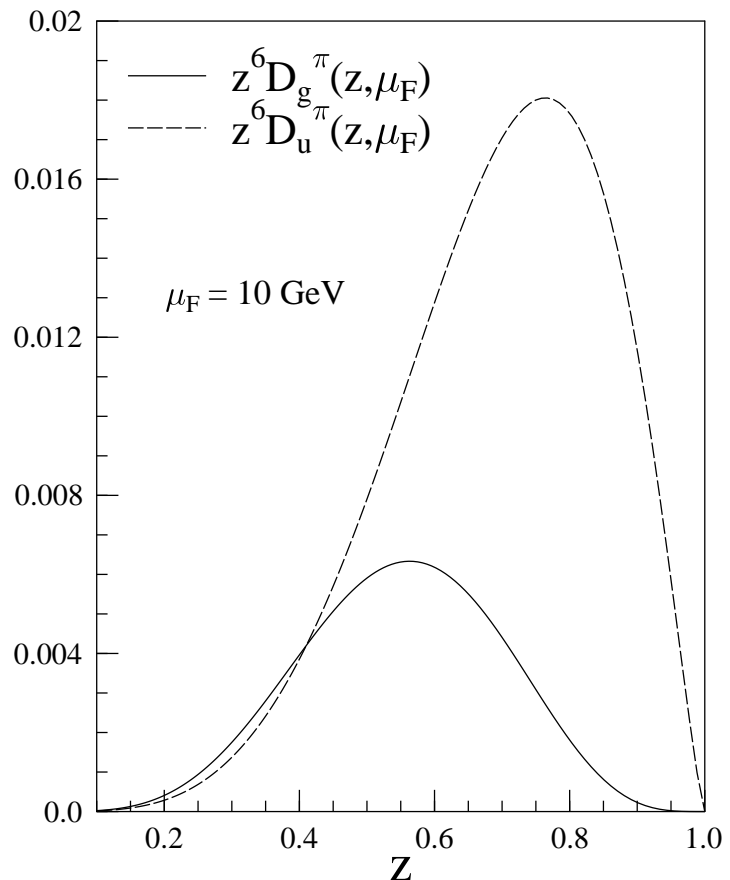


Figure 12: The integrand of Eq. (19) with  $n = 7$ . The fragmentation functions are from KKP [4]. The integrand is peaked at  $\bar{z}_f$ .

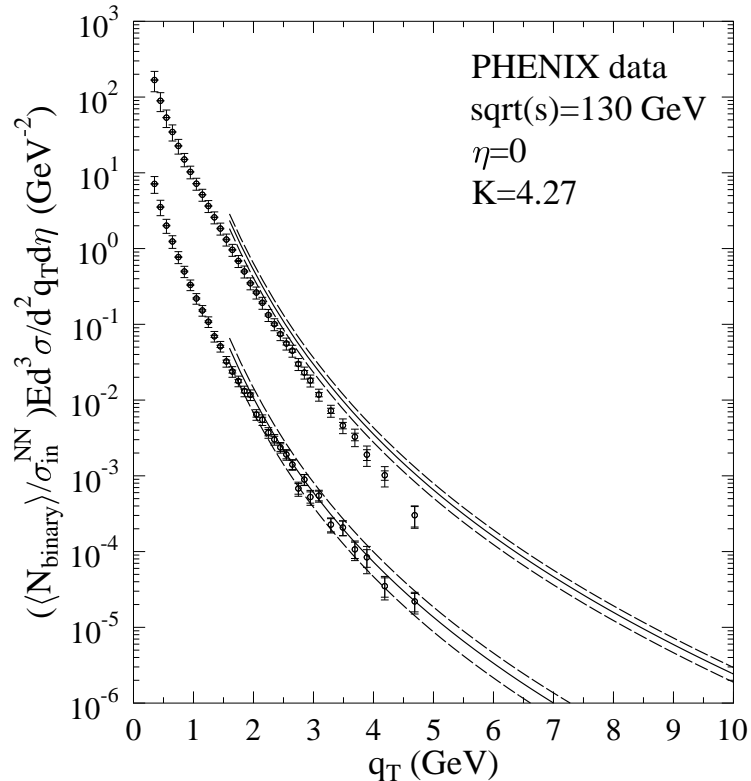


Figure 13: Charged-hadron spectra for centrality classes 0...10% and 60...80% in Au+Au collisions at  $\sqrt{s} = 130$  AGeV at RHIC. The data are from PHENIX [17]. The solid curves are the pQCD results computed with  $K = 4.27$  and  $A_{\text{eff}} = 163$  and 9 for the two centrality selections. The error bands shown by the dashed lines correspond to an estimated total uncertainty of  $\pm 22\%$  and  $\pm 36\%$ , respectively (see the text).